JACS
JOURNAL OF THE AMERICAN CHEMICAL SOCIETY

ARTICLE

pubs.acs.org/JACS

Dimerization of HNO in Aqueous Solution: An Interplay of Solvation Effects, Fast Acid−Base Equilibria, and Intramolecular Hydrogen Bonding?

Carsten Fehling* and Gernot Friedrichs*

Institut für Physikalische Chemie, Christian-Albrechts-Universität zu Kiel, Olshausenstraße 40, 24098 Kiel, Germany

Supporting Information

ABSTRACT: The recent unraveling of the rather complex acid−base equilibrium of nitroxyl (HNO) has stimulated a renewed interest in the significance of HNO for biology and pharmacy. HNO plays an important role in enzymatic mechanisms and is discussed as a potential therapeutic agent against heart failure. A cumbersome property for studying HNO reactions, its fast dimerization leading to the rapid formation of N_2O, is surprisingly far from being well understood. It prevents isolation and limits intermediate concentrations of nitroxyl in solution. In this study, a new mechanism for the HNO dimerization reaction in aqueous solution has been theoretically derived on the basis of DFT calculations. Detailed analysis of the initial reaction step suggests a reversal of the *cis*−*trans* isomer preference in solution compared to the corresponding gas phase reaction. In contrast to a gas phase derived model based on intramolecular rearrangement steps, an acid−base equilibrium model is in agreement with previous experimental findings and, moreover, explains the fundamental differences between the well studied gas phase reaction and the solvent reaction in terms of polarity, *cis*−*trans* isomerizations, and acidities of the intermediates. In the case of *cis*-hyponitrous acid, the calculated pK_a values of the acid−base equilibria were found to be significantly different from the corresponding experimental value of the stable *trans* isomer. Under physiological conditions, N_2O formation is dominated by the decomposition of the unstable monoanion *cis*-$N_2O_2H^-$ rather than that of the commonly stated *cis*-HONNOH.

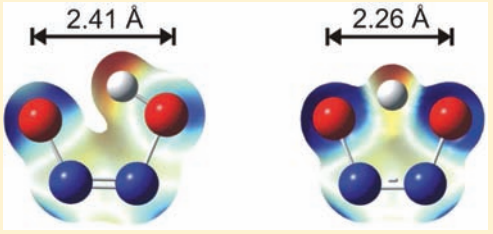

1. INTRODUCTION

The interest in the chemistry of nitroxyl (HNO) in solution has rapidly increased owing to two important findings that have led to a reevaluation of the significance of HNO among the nitrogen species in physiologically and biologically relevant systems.[1] First, the previously reported pK_a value of nitroxyl, pK_a = 4.2, has been redetermined by both experiment and theory and has been corrected to the dramatically different value 11.4.[2,3] The second important issue was the reassessment of the HNO dimerization rate constant in solution, which was found to be on the order of 8×10^6 M^{-1} s^{-1} and thus significantly lower than the previously reported nearly diffusion limited value of 2×10^9 M^{-1} s^{-1}.[2] The much longer lifetime of HNO in aqueous solution and its certain stability under physiologically relevant conditions enables reactions in solution prior to the dimerization reaction itself. Experimental studies revealed a reaction selectivity of HNO that deviates strongly from that of NO. For example, HNO reacts rapidly and selectively with thiols, whereas NO requires activation by species enabling its oxidation, e.g., transition metals.[4] The unique chemistry combined with the low radius of action of freshly generated HNO has led to a discussion about possible site specific biological effects and the use of potential chemical HNO sources as pharmaceutical agents.[1] However, the observation of DNA strand breakage in the presence of HNO, which is more strongly induced under acidic conditions (pH < 6), has been suggested as evidence for a strong oxidative capability.[5] This unfavorable property was later attributed to the formation of OH radicals from a side reaction of HNO dimerization.[6]

Besides this pharmaceutical interest, direct HNO dimerization was postulated as a chemical pathway for nitrous oxide formation from nitrous oxide reductase (NOR) enzymes found in nitrifying and denitrifying bacteria and fungi. Although new insights into the corresponding NOR enzyme mechanism underlined that the N−N bond formation takes place at the active site of the enzyme and is catalyzed by a binuclear iron complex, the role of HNO reactions in several enzyme mechanisms, especially due to its high affinity to transition metal complexes, remains unclear.[7]

Despite its importance and many experimental studies of this reaction,[2,8−10] the detailed mechanism of the HNO dimerization in solution is poorly understood. Because of rapid sequential isomerization steps and proton transfer reactions, often N_2O formation itself is the only accessible experimental indicator for the ongoing reaction sequence.[1] Typically, hyponitrous acid is stated as the crucial intermediate species that decomposes to form nitrous oxide:

$$HNO + HNO \rightarrow [HONNOH] \rightarrow N_2O + H_2O \qquad (1)$$

Received: August 11, 2011
Published: October 17, 2011

dx.doi.org/10.1021/ja2075949 | *J. Am. Chem. Soc.* 2011, 133, 17912–17922

Whereas the kinetics of the overall reaction were found to be second order with respect to HNO concentration in pulse radiolysis and flash photolysis studies,[2] to the best of our knowledge neither has the assignment of *cis*-hyponitrous acid as intermediate been experimentally verified nor does a valid mechanism for the overall reaction sequence in solution exist. In the case of Angeli's salt (sodium α-oxohyponitrite), a widely used chemical HNO source, several isotope labeling studies revealed that N-protonation to $O^{15}N(H)^{14}NO_2$ and the subsequent decomposition form isotopically pure $^{15}N^{15}NO$.[11] The initially formed N−N bond of the HNO dimer is therefore generally believed to be preserved in a sequence of unimolecular reactions eventually forming N_2O.

Several experimental and theoretical studies have been performed to clarify the mechanism of the gas phase recombination reaction.[12,13] The temperature dependence of the rate constant indicates a small activation barrier on the order of $E_0 \approx 4-14$ kJ/mol and a low preexponential Arrhenius factor of about 1×10^9 cm^3 mol^{-1} s^{-1}.[12,13] The latter is in accordance with a high entropy of activation and thus a highly ordered transition state.[12] Attempts were made to model the complete scheme of sequential reactions on the basis of *ab initio* calculations assuming *trans*-ON(H)N(H)O as the initial dimer species. In agreement with other quantum chemical models,[14,15] the *trans*-ON(H)N(H)O isomer has been found to be significantly more stable than the *cis*-ON(H)N(H)O isomer. Consequently, the formation and further reactions of the *cis* isomer have been neglected.

Despite these sound schemes and measurements of the reaction in the gas phase, some obscurities remain for the reaction in solution. First of all, the initial reaction is faster in solution (8×10^6 M^{-1} s^{-1})[2] than it is in the gas phase ($0.5-1.6\times 10^6$ M^{-1} s^{-1}).[12] Second, the final decomposition step leading to the formation of nitrous oxide has been assigned to different tautomers and isomers in the literature.[12,14,16] Furthermore, most experimental studies agree on stoichiometric and fast nitrous oxide generation from HNO dimerization in solution,[17,18] whereas theoretical gas phase studies report *trans*-hyponitrous acid formation as an intermediate or byproduct.[12] Of course, the results of gas phase studies cannot be directly compared with the outcome of the reaction in solution. For the gas phase reaction, energy conservation has been assumed for the initial dimer and subsequent intermediates, thus allowing for rapid crossing of the involved reaction barriers.[12,14] In contrast, fast collisional deactivation of the energetically excited initial adduct takes place in solution, resulting in stabilization of the dimer and possibly much different overall kinetics.

The aim of this work is to provide a theoretical backbone to explain the diverging experimental results and mechanistic interpretations in a unified model. Following a more detailed analysis of the initial dimerization reaction, an existing gas phase mechanism relying on intramolecular rearrangement steps has been tested with regard to its applicability on the reaction in solution. In DFT based calculations, solvent effects have been taken implicitly into account by applying polarization continuum models and, in some cases, explicit solvent molecules have been included to allow for solvent based catalysis. Detailed analysis of possible isomerization steps as well as the involvement of ionic species led to the development of a mechanistic model based on fast acid−base equilibria. Theoretically derived pK_a values were used to deduce the most feasible reaction pathways. The predicted product yields and pH dependencies are critically compared with the identified products of previous experimental studies, showing that the proposed mechanism is consistent with the reported, sometimes controversially discussed literature findings.

2. COMPUTATIONAL METHODOLOGY

Quantum chemical calculations were performed utilizing the Gaussian 09 program suite.[19] If not stated otherwise, DFT calculations presented in this study were based on the B3LYP functional using Dunning's correlation consistent aug-cc-pVTZ basis set.[20] Solvation effects were taken into account by the polarization continuum models CPCM and IEFPCM using UFF cavities.[21] After optimization, harmonic frequency analysis revealed minimum and transition state (TS) structures (zero and one imaginary frequency, respectively). TS structures were checked to connect the respective minimum structures by following the intrinsic reaction coordinates.

To derive accurate theoretical pK_a values within Δp$K_a = \pm 1$, the concept of proton exchange was applied.[22] In this scheme, a structurally similar acid (HRef) is used as internal reference such that the error-prone solvation energy of the proton is not required:

$$HX + Ref^- \rightleftharpoons X^- + HRef \qquad (2)$$

The pK_a value of the acid of interest is deduced from free enthalpies of solution and the corresponding experimental pK_a value of the reference acid:

$$pK_a = \frac{\Delta G^*_{soln}}{RT\ln(10)} + pK_a(HRef) \qquad (3)$$

The free enthalpy of the reaction in solution ΔG^*_{soln}(standard state 1 mol/L) is determined from a valid thermodynamic cycle consisting of the gas phase enthalpy of reaction, ΔG^*_{gas} and contributions of the free enthalpies of solvation compared to the products and educts.

$$\Delta G^*_{soln} = \Delta G^*_{gas} + \sum_{products} \Delta G^*_{solv} - \sum_{educts} \Delta G^*_{solv} \qquad (4)$$

trans-Hyponitrous acid was chosen as a suitable reference acid. It is fairly stable in solution such that standard titration experiments could be used to determine $pK_{a,1} = 7.18$ and $pK_{a,2} = 11.54$ for the first and the second deprotonation, respectively.[23]

3. RESULTS AND DISCUSSION

3.1. Initial Dimerization in Solution. The initial dimerization of HNO forming the *trans* or *cis* isomer sets the starting point for the reaction sequence. As will be discussed in more detail below, the initial isomer preference turns out to define the overall product formation pathway. Once formed, *cis*−*trans* isomerization cannot take place due to significant energy barriers. In order to comprehend the isomer preference of the reaction in solution, a few structural considerations are necessary.

Thermodynamic Equilibrium. The DFT calculations show that introducing a solvent cage in terms of the polarization continuum model leads to quite different stabilizations of the involved *cis* and *trans* species (**2**,**3**). Selected free enthalpies of solvation, the dipole moments, and the calculated equilibrium constants are listed in Table 1. Here, the results both of the standard UFF cavity parametrization and of the rather novel SMD model[24] are shown in comparison to emphasize the uncertainties associated with the description of solute parameters in highly dielectric media such as water. For example, the changes of dipole moments and the solvent enthalpies of the highly dipolar species deviate significantly. However, the overall trends

Table 1. Dipole Moments, μ, Free Enthalpies of Solvation, ΔG^*_{solv}, and Free Enthalpies Relative to the Educt HNO in the Gas Phase, ΔG^*_{gas}, and in Solution, ΔG^*_{soln}[a]

				IEFPCM (UFF)			IEFPCM (SMD)	
species		μ_{gas}	ΔG^*_{gas}	μ_{soln}	ΔG^*_{solv}	ΔG^*_{soln}	μ_{soln}	ΔG^*_{solv}
HNO	**1**	1.65		2.07	−9.9		2.29	−10.8
2 × HNO	**1**		0.0		−19.8	0.0		−21.6
cis-ON(H)N(H)O	**2**	5.45	−46.7	7.20	−57.2	−84.5	8.04	−110.9
trans-ON(H)N(H)O	**3**	0.00	−53.3	0.00	−34.2	−68.3	0.00	−61.0
TST *trans*-ON(H)N(H)O	**1** → **3**	0.00	34.8	0.00	−18.5	36.0	0.00	−11.0

[a] Calculations are based on the polarization continuum models IEFPCM(UFF) and IEFPCM(SMD). Units are Debye and kJ/mol.

are similar such that the conclusions drawn from the two different solvent models are identical.

The main contributions for stabilization in solution stem from electrostatic interactions originating from changes of polarity and polarizability of the solute. As already discussed by Glaser et al.,[25] the two dipole moment vector components cancel in the case of the *trans* dimer (**3**), whereas for the *cis* dimer (**2**) the net dipole moment is even larger than the sum of the dipole moments of the two HNO monomers. Due to the structural adjustment of the equilibrium geometry in dielectric media, the magnitude of the net dipole moment is further increased. Thus, dipole−dipole interactions contribute significantly to the *cis* dimer (**2**) stabilization in aqueous solution. In contrast, the stabilization of the *trans* dimer (**3**) compared to the monomer is rather an effect of increased polarizability of the dimer species and increased polarity due to the shift of electron density along the N−O bond toward oxygen. These effects are basically independent of the isomer structure and thus equally contribute to the stabilization of the two isomers. Overall, due to the large difference in free enthalpies of solvation between the *cis* and *trans* dimers, the thermodynamic preference of the *trans* dimer (**3**) in the gas phase is more than compensated such that the *cis* species (**2**) is more stable in solution.

Solvent Effect on Long-Range Interactions. The question arises how the rate constants of the dimer formation are affected by the solvent. In comparison with the gas phase reaction, effects might originate from different contributions of long-range interactions such as hydrogen bonding and dipole−dipole interactions. Peters[26] has shown for the gas phase species that intermolecular hydrogen bonding can stabilize metastable *trans*-like dimer structures by ≈9 kJ/mol at N−N distances around 2.5 Å. In addition, using the dipole moment stated in Table 1, the dipole−dipole interaction energies at this distance and for a parallel orientation can be estimated to be on the order of 2−4 kJ/mol. This interaction is attractive in the case of a *trans* orientation and repulsive in the case of the *cis* orientation. Both types of interaction are thus in favor of *trans* dimer formation in the gas phase. However, comparing these long-range HNO−HNO interaction energies with the calculated solvation enthalpies of two HNO molecules (>20 kJ/mol) reveals that in aqueous solution the solute−solvent dipole−dipole and hydrogen bonding interactions dominate. In other words, the long-range interactions are shielded by solvation shells and thus can be assumed to play no significant role for the reaction in solution.

Solvent Effect on Bond Formation. At shorter N−N distances (<2.0 Å), on the one hand, energetic stabilization takes place due to mutual $n(N') \rightarrow \pi^*(N-O)$ orbital interactions (finally leading to σ- and π-(N−N) bond formation). On the other hand, repulsive interactions originate from the proximity of nitrogen and oxygen lone pairs. In fact, our own DFT calculations revealed a transition state structure for the *trans* species (**3**) formation, but with no significant energy barrier relative to the HNO molecules. This result is contrary to earlier theoretical studies[15,14] reporting an energy barrier up to 45 kJ/mol, but it is in line with the MP4 results of Lin et al.[12] The experimental temperature dependence of the rate constant in the gas phase also suggests a low dimerization barrier for *trans* dimer (**3**) formation of merely 4−14 kJ/mol.[13,27] Furthermore, the low preexponential Arrhenius factor found in the experiments and the calculated free enthalpy differences underline the formation of a free enthalpy barrier. Instead of enthalpy it is the strong decrease of entropy during the reaction that determines the overall rate.

As a result of the strongly exothermic character of the reaction, the rate determining free enthalpy maximum is located at the early bond formation stage. From the DFT gas phase model, a rough estimate of the corresponding N−N distance of 1.7 Å was obtained. Due to the strong stabilization of the products in solution, this maximum can be assumed to shift even further outward. At this early stage of the reaction, only a minor change of polarizability and polarity of the NO bond has taken place. In contrast, as a result of the required relative orientation of the two HNO fragments, the net dipole moment has already vanished for *trans* dimer formation but has increased or at least has been preserved for *cis* dimer formation. Thus, it can be expected that formation of the dipolar *cis* dimer is preferred due to the solvent effect.

Rate Increase in Solution. In the gas phase, overall HNO dimerization reaction rate constants of $0.5-1.6 \times 10^6\ M^{-1}\ s^{-1}$ have been determined and theoretical isomer specific rate constants predict an initial isomer ratio of 3 to 1 in favor of the *trans* adduct (**3**).[12,13] The recently reported aqueous phase rate constant,[2] $8 \times 10^6\ M^{-1}\ s^{-1}$, is significantly higher than the gas phase rate constant, but it is still well below the diffusion limit. Shafirovich and Lymar[2] related this rate enhancement in solution to the free enthalpy of solvation of HNO by implicitly assuming similar free enthalpies of solvation of HNO and the activated complex. However, in light of the distinct dipole moment changes taking place during the reaction, this assumption is questionable. Instead, the overall solvent effect on the rate constant, $\Delta_{solv}\Delta G^{\ddagger}$, has to be dissected into contributions of reactant and transition state free enthalpies of solvation, ΔG^R_{solv} and $\Delta G^{\ddagger}_{solv}$, according to[28]

$$\Delta_{solv}\Delta G^{\ddagger} = \Delta G^{\ddagger}_{solv} - \Delta G^{R}_{solv} \quad (5)$$

Considering the loss of dipole moment and with it a relative increase of the transition state barrier in the case of the *trans*

dimer (**3**), it appears unlikely that the observed rate constant enhancement in solution originates from this pathway. In contrast, the better stabilization of the transition state structure of the *cis* dimer (**2**) is expected to considerably change the ratio of the formed isomers.

A quantitative description of solvent effects based on solute−solvent dipole−dipole interactions can be based on the theoretical model given by Kirkwood.[29] Along those lines, by taking into account dipole moment stabilization on the free enthalpy of activation, it is possible to estimate the change of rate constants going from the gas phase to the solution.[28] Assuming that the change of dipole moment is the dominating effect and the additional solvent specific effects such as hydrogen bonding are similar for the two isomers, the change of the isomer ratio of the initial HNO dimerization rate constants can be obtained from the following:

$$\frac{k_{cis,\,\mathrm{soln}}}{k_{trans,\,\mathrm{soln}}} = \frac{k_{cis,\,\mathrm{gas}}}{k_{trans,\,\mathrm{gas}}} \exp\left(\frac{1}{4\pi\varepsilon_0}\frac{1}{k_B T}\left(\frac{\varepsilon_r - 1}{2\varepsilon_r + 1}\right)\left(\frac{(\mu_{cis}^{\ddagger})^2}{r_{cis}{}^3} - \frac{(\mu_{trans}^{\ddagger})^2}{r_{trans}{}^3}\right)\right) \quad (6)$$

Here, ε_r is the dielectric constant of the solvent, $\mu_i^{\ddagger}$ is the transient dipole moment of the molecular structure corresponding to maximum free enthalpy, and r_i is the effective radius of the dimer complex in solution. The expression provides a lower limit for the estimated change of the isomer ratio, since the effects in highly dielectric media such as water are underestimated. With an effective dipole moment of ≈4.5 D, a calculated effective radius of 3.2 Å for the structure corresponding to the maximum free enthalpy of the *cis* dimer complex, and a negligible dipole moment of the *trans* dimer ($\mu_{trans}^{\ddagger} = 0$), the exponential term in eq 6 accounts for a factor of 1500. Combining this number with the reported 3-fold isomer preference in the gas phase, an overall isomer ratio in solution of $k_{cis,\mathrm{soln}}/k_{trans,\mathrm{soln}} = 500$ is predicted, hence strongly in favor of the *cis* isomer. Similarly, using a calculated effective radius of 2.9 Å for the HNO monomer, the equivalent equation for $k_{cis,\mathrm{soln}}/k_{cis,\mathrm{gas}}$ predicts a rate constant increase of approximately 30 for *cis* dimer (**2**) formation in solution. Again, taking into account the stated 3-fold *trans* isomer preference in the gas phase, this yields an approximately 8-fold increase of the overall rate constant—in very good agreement with the experimental 14-fold rate enhancement found in solution.

In summary, due to additional stabilization effects arising from dipole−dipole interactions and in contrast to the gas phase result, the *cis* dimer (**2**) can be considered to be the by far more favorable adduct in solution.

3.2. Impact of Solvation on Sequential N_2O Formation. The change of the initial isomer ratio raises the question if the previously discussed sequential gas phase reaction models[12,14] result in feasible N_2O formation pathways in solution as well. In the simplest case, the sequential gas phase and solvent mechanisms are equivalent and the influence of the solvent on the overall energetics would give a valid explanation of the much more rapid formation of N_2O in solution compared to the gas phase. In this section, the effects of solvation have been treated implicitly and explicitly to investigate this hypothesis.

Implicit Solvent Effect. Starting from the gas phase reaction schemes reported in the literature,[12] the implicit effect of the solvent on the energies of possible intermediates and transition state structures has been determined by applying the IEFPCM-(UFF) solvent model. The resulting reaction path diagram is shown in Figure 1. The corresponding structures and energies are listed in the ESI.

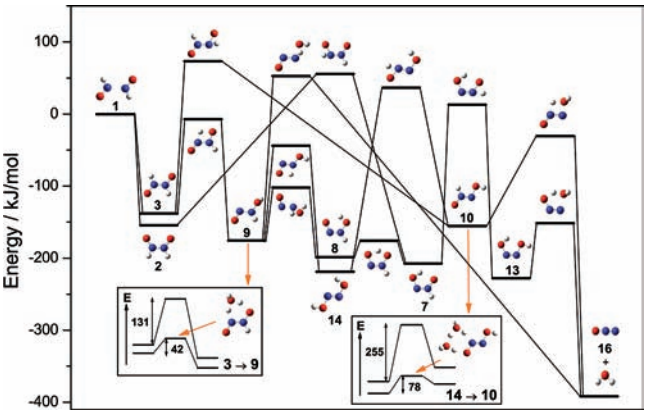

Figure 1. Implicit and explicit (inset) solvation effects on the intermediate species assuming the gas-phase model for HNO dimerization. Shown energy levels represent the electronic energies of the optimized ground state and transition state structures in solution relative to the educt energies. The two insets illustrate transition state structures including catalytically active explicit water molecules resulting in significant decreases of the corresponding activation energies due to hydrogen bonding. As outlined in the text, none of the shown pathways (although thermodynamically feasible) reflect the experimental result of rapid nitrous oxide formation in solution adequately.

It turns out that, except for the initial dimer, in comparison with the gas phase scheme, only small changes of the relative energies arise such that the mechanism remains thermodynamically feasible and the main possible pathways are similar to the gas phase reaction mechanism as discussed by Lin et al.[12] Besides the possible *cis*−*trans* isomerization **9** → **8**, basically 1−3 and 1−2 hydrogen shifts are involved in N_2O formation.

$$trans\text{-}\mathrm{ON(H)N(H)O}\ (\mathbf{3}) \rightarrow \mathbf{9} \rightarrow \mathbf{8} \rightarrow \mathbf{7} \rightarrow \mathbf{13} \rightarrow \mathbf{16} \qquad E_0^{\max} = 220\ \mathrm{kJ/mol} \quad (7)$$

$$\rightarrow \mathbf{10} \rightarrow \mathbf{16} \qquad E_0^{\max} = 210\ \mathrm{kJ/mol} \quad (8)$$

$$\rightarrow \mathbf{9} \rightarrow \mathbf{16} \qquad E_0^{\max} = 230\ \mathrm{kJ/mol} \quad (9)$$

$$\rightarrow \mathbf{9} \rightarrow \mathbf{14} \rightarrow \mathbf{10} \rightarrow \mathbf{16} \qquad E_0^{\max} = 255\ \mathrm{kJ/mol} \quad (10)$$

$$cis\text{-}\mathrm{ON(H)N(H)O}\ (\mathbf{2}) \rightarrow \mathbf{7} \rightarrow \mathbf{13} \rightarrow \mathbf{16} \qquad E_0^{\max} = 220\ \mathrm{kJ/mol} \quad (11)$$

Here, $E_0^{\max}$ specifies the highest occurring barrier for each reaction pathway. Note, that the reaction pathways according to eqs 7 and 11 correspond to the commonly cited scheme via *cis*-hyponitrous acid (**13**). In principle, eq 10 could serve as an explanation for the formation of *trans*-hyponitrous acid (**14**) in the reaction sequence, as predicted for the gas phase reaction. With $E_0^{\max} > 200$ kJ/mol for all possible reaction pathways, the reaction barriers are way too high to be consistent with a rapid reaction found in the experiment. A possible reason for this discrepancy might be that the influence of the solvent is not reflected adequately by the simple change of the dielectric constant assumed in the polarization continuum model. Additional stabilization by means of hydrogen bonds is not described by such an implicit modeling approach.

Explicit Solvent Effect. Therefore, in a next step, we explicitly included single solvent molecules in the reactions. A similar approach was recently presented by Ashcraft et al.[30] to determine the rate constants of hydroxylamine oxidation in nitric acid, which is largely comparable to the scheme presented here.

dx.doi.org/10.1021/ja2075949 |J. Am. Chem. Soc. 2011, 133, 17912–17922

Table 2. Theoretical Solvent Free Energies and Reaction Barriers in kJ/mol and p*K* Values for Isomerization Equilibria Determined Using the IEFPCM(UFF) Model[a]

reaction				equilibrium			TST	
educt		product		$\Delta(\Delta G^*_{solv})$	$\Delta_r G^*_{soln}$	p*K*	$\Delta E^{\ddagger}_{soln}$	$\Delta G^{\ddagger}_{soln}$
trans-ON(H)N(H)O	**3**	*cis*-ON(H)N(H)O	**2**	−23.1	−16.3	−2.85	n.a.	n.a.
trans-ON(H)NO$^-$	**5**	*cis*-ON(H)NO$^-$	**4**	−16.3	−11.3	−1.98	172.0	164.5
trans-HON(H)NO	**9**	*cis*-HON(H)NO	**8**	4.8	−21.3	−3.73	78.0	73.4
trans-HONN(H)O	**10**	*cis*-HONN(H)O	**7**	6.9	−24.2	−4.23	242.0	241.7
trans-ONNO^{2-}	**11**	*cis*-ONNO^{2-}	**6**	−17.8	1.6	0.28	n.a.	n.a.
trans-HONNO$^-$	**15**	*cis*-HONNO$^-$	**12**	8.8	−32.2	−5.71	232.2	226.0
trans-HONNOH	**14**	*cis*-HONNOH	**13**	1.8	−9.2	−1.61	n.a.	n.a.

[a] The label "n.a." indicates that bond dissociation was found to be energetically more favorable. In those cases, relaxed potential energy scans were performed showing that barriers of at least 200 kJ/mol are involved.

In agreement with their results, the reaction barriers for the 1−3 hydrogen shift reactions were found to be significantly lowered when a single water molecule was included. As shown in the left inset of Figure 1, the water molecule forms a six membered ring structure that is geometrically and energetically favorable and catalyzes the hydrogen atom transfer. The corresponding reaction barrier decreases from 131 to 42 kJ/mol. In the case of 1−2 hydrogen shifts, the resulting five membered ring structure is geometrically too demanding, but analogous stabilizations of the transition state barriers were found by allowing for two explicit water molecules instead (e.g., right inset of Figure 1).

In contrast, we were unable to locate similarly stabilized structures for the reactions **9** → **16** and **10** → **16**. In these cases, the proton transfer is coupled with the dissociation and hydrogen bond structures are less stable due to the lower charge at the involved oxygen atom. Consequently, the direct elimination of water from the intermediates (**9**, **10**) remains energetically unfeasible and a major contribution of these pathways to nitrous oxide formation appears unlikely.

Surprisingly, no stabilization was found for the calculated transition state structure of the reaction **7** → **13** as well—in contrast to the analogous reaction of the *trans* isomer **10** → **14**. The corresponding formation of *cis*-hyponitrous acid (**13**) is crucial, however, for N_2O formation both from the *trans* dimer (**3**) according to eq 7 and from the preferred *cis* dimer (**2**) in eq 11. It is interesting to note that this important reaction step has been neglected in recent reaction schemes, although significant barriers are involved.[30,31] Instead, Raman et al.[31] implicitly assumed a fast *cis*−*trans* isomerization from **14** to **13**. As will be discussed below, such an isomerization step is unfeasible.

In summary, in the presented intramolecular reaction scheme, both excluding and including explicit water, at least one elementary step within the N_2O formation reaction sequence involves kinetically unfavorable high energy barriers. Although *cis*-hyponitrous acid (**13**) has been assumed throughout the literature as the principle species decomposing rapidly to form nitrous oxide, neither the simple solution model nor the inclusion of catalytically acting water molecules reveal possible pathways to the formation of the *cis*-hyponitrous acid (**13**) intermediate. Note, however, that the reaction sequence remains energetically downhill and thus is thermodynamically feasible. Moreover, certain intramolecular proton transfer reactions with low barriers (e.g., **8** → **7**) can play a role, and catalytically acting water can lower reaction barriers quite significantly such that reactions such as **3** → **9** become feasible in aqueous solution. Finally, the intramolecular scheme reveals that the often discussed, simple decomposition of the molecular species (**9**, **10**, **13**)[12,14,16] into nitrous oxide is inaccessible or very slow.

3.3. Isomerization and *cis*−*trans* Equilibria. Failure of the straightforward sequential reaction scheme discussed in the previous section calls for alternative reaction models. So-far neglected options are inclusion of possible *cis*−*trans* isomerizations and dissociation into ionic species. In this section, the first option will be discussed in connection with the involved activation barriers and the thermodynamic equilibria of the shown isomers and related ionic species. The isomerization equilibria reflect the impact of the isomer structure on inter- and intramolecular interactions, revealing the differences in dissociation behavior of the isomers.

Isomerization Barriers. Additional interconnecting *cis*−*trans* isomerization pathways could originate from one of the various intermediates shown in Figure 1. Such isomerizations around N−N bonds with more or less double bond character have been discussed to take place in quite similar reaction sequences of hydroxylamine oxidation in nitric acid[32] and decomposition of *trans*-hyponitrous acid.[33] Transition state optimizations and relaxed potential energy scans along the ONNO-dihedral angle have been performed. Calculated equilibria and reaction barriers of the relevant transient species are shown in Table 2. Related deprotonated species are included in the table as well. They become important for the acid-basis scheme discussed in the next section. In some cases (labeled "n.a." in Table 2), bond dissociation was found to be energetically more favorable than isomerization, and hence, no transition state is specified.

All isomerization steps, except HON(H)NO (**9**) → **8**, with a barrier of ΔE_{soln} = 78 kJ/mol, exhibit energy barriers of at least 172 kJ/mol and are, thus, too high to be accessible at room temperature conditions. Moreover, the free enthalpies of reaction clearly point out that the thermodynamics are in favor of the *cis* species. The only exception is the dianion (**6**, **11**), which is slightly more stable in its *trans* form.

Thermodynamic Stability. As already discussed for ON(H)N(H)O (**3**), the electrostatic interaction of the solvent favors the molecules with higher dipole moments. For the N-protonated anion (**5**) and the dianion (**11**), solvation effects shift the thermodynamic equilibrium toward the *cis* isomers, as apparent from the large differences of the free enthalpy of solvation, $\Delta(\Delta G^*_{solv})$. On the contrary, for the O-protonated species with $\Delta(\Delta G^*_{solv}) > 0$, the origin of the isomeric preference changes. Here, intramolecular hydrogen bonding leads to an additional

stabilization of the *cis* isomers in the case of **7**, **8**, and **12**. An exception is *cis*-hyponitrous acid (**13**), for which Zevallos et al.[34] pointed out that the higher thermodynamic stability is related to an electronic effect (favorable LP(N′) → σ^*(N−O) orbital interactions) rather than the weak intramolecular hydrogen bonding. The same interaction, even so less pronounced, is present in the case of the anion (**12**) and the dianion (**6**) and leads to a significant decrease of kinetic stability with respect to dissociation forming N_2O. Due to the increasing N−N bond length and decreasing LP(N′) → σ^*(N−O) overlap, this effect decreases in the order *cis*-hyponitrous acid (**13**), *cis*-hyponitrite monoanion (**12**), and *cis*-hyponitrite dianion (**6**).

The very high stability of the single ionic species *cis*-HON-NO$^-$ (**12**) in comparison with that of its *trans* isomer (**15**) turns out to play a key role in the following acid−base equilibria and requires a more detailed discussion. The electrostatic potential of the optimized cyclic structure of **12** (see Figure 2) suggests contributions of intramolecular hydrogen bonding to the stabilization of the cyclic *cis* isomer. Indeed, although better stabilized in solution, the alternative *cis* conformer with an exocyclic hydrogen atom is calculated to be 22.6 kJ/mol more endergonic. In addition to this, the intramolecular proton transfer can be considered to be very fast due to a low free energy of activation in solution of merely 6.4 kJ/mol. The corresponding symmetric structure of the transition state is shown in Figure 2. An important aspect of the illustrated structures is the unusually short distance between the oxygen atoms, often used for classifying hydrogen bonds.[35] The calculated short distances between the oxygen atoms in the anion, 2.41 Å, and in the transition state, 2.26 Å, as well as the equivalent donor−acceptor capabilities and the favorable geometry formally meet the criteria of a so-called low-barrier hydrogen bond (LBHB). Often closely linked to these structures is an increasing difference of the acid-dissociation constants ΔpK_a as known from the acid−base chemistry of maleic acid. A similar influence on the protonation equilibrium of *cis*-hyponitrous acid is expected and will be discussed in more detail below.

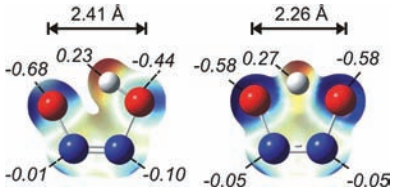

Figure 2. Optimized structures of the *cis*-hyponitrite anion (left) and the transition state (right) corresponding to the intramolecular hydrogen transfer. Highlighted are the electrostatic potentials color coded, the partial charges (in italic letters), and the unusually short O−O distance in the transition state.

To summarize the findings of this section, on the one hand, isomerizations are unlikely to play a role for the overall reaction scheme leading to N_2O formation from HNO dimerization. On the other hand, ionic species show remarkable stabilization effects in solution and therefore could play a so-far overlooked major role.

3.4. Acid−Base Equilibrium Scheme. Stimulated by the results of the preceding section and similar to an approach presented by Dutton et al.[36] for Angeli's salt decomposition, an acid−base equilibrium based reaction scheme for N_2O formation from HNO dimerization has been worked out. Including the ionic species in the reaction mechanism in solution is based on the assumption that acid−base equilibration of the relevant species is fast. The new scheme for the HNO dimerization is shown in Figure 3. The numbers in parentheses refer to calculated pK and pK_a values, and the latter are summarized again in Table 3.

Acid−Base Equilibria. In aqueous solution, for both the *cis* and *trans* pathways, rapid deprotonation of the initial dimer species (**2**, **3**) leads to the formation of the N-protonated ions (**4**, **5**). In the next step, under moderately *acidic* conditions, O-protonation is more favorable than a second deprotonation. Regarding the

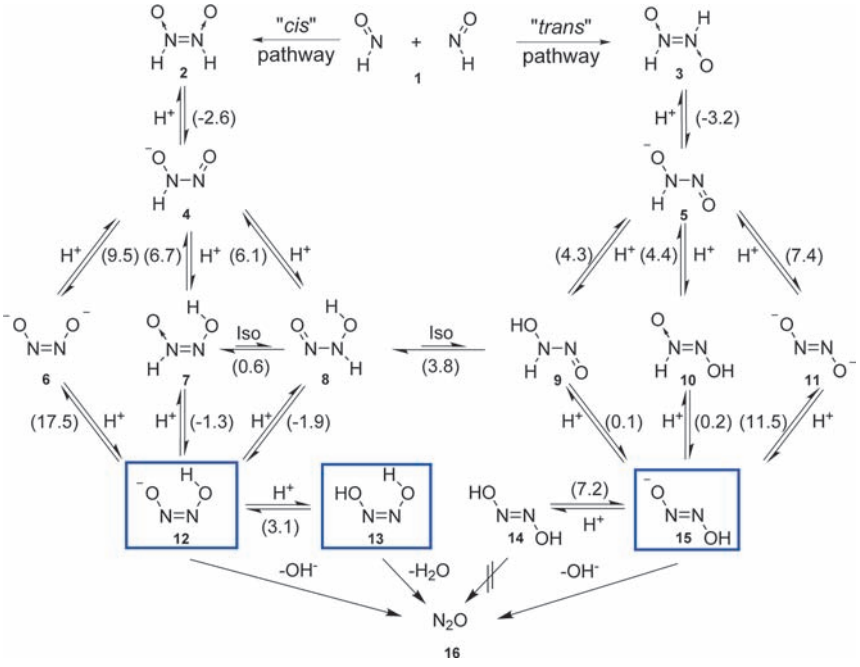

Figure 3. Acid−base equilibria model for the HNO dimerization reaction. The numbers in parentheses represent pK_a values as determined from eq 3 and pK values in the case of isomerization reactions. The species marked with frames are unstable with respect to decomposition yielding nitrous oxide.

dx.doi.org/10.1021/ja2075949 |*J. Am. Chem. Soc.* 2011, 133, 17912–17922

Table 3. Theoretically Calculated Free Enthalpies of Reaction ΔG^*_{soln} in Solution (in kJ/mol, T = 298 K) and pK_a Values, Both Referenced to the Stated Acid−Base Equilibria HRef1 and HRef2

equilibrium				IEFPCM(UFF)		CPCM(UFF)	
acid		base		ΔG^*_{soln}	pK_a	ΔG^*_{soln}	pK_a
cis-ON(H)N(H)O	**2**	*cis*-ON(H)NO$^-$	**4**	−56.4	−2.6	−56.7	−2.7
cis-HON(H)NO	**8**	*cis*-ON(H)NO$^-$	**4**	−6.5	6.1	−7.1	5.9
cis-HON(H)NO	**8**	*cis*-HONNO$^-$	**12**	−52.1	−1.9	−52.4	−1.9
cis-HONN(O)H	**7**	*cis*-ON(H)NO$^-$	**4**	−3.0	6.7	−3.4	6.6
cis-HONN(O)H	**7**	*cis*-HONNO$^-$	**12**	−48.6	−1.3	−48.7	−1.3
cis-HONNOH	**13**	*cis*-HONNO$^-$	**12**	−23.4	3.1	−23.6	3.1
trans-ON(H)N(H)O	**3**	*trans*-ON(H)NO$^-$	**5**	−59.7	−3.2	−59.9	−3.3
trans-HON(H)NO	**9**	*trans*-ON(H)NO$^-$	**5**	−16.7	4.3	−16.4	4.3
trans-HON(H)NO	**9**	*trans*-HONNO$^-$	**15**	−40.7	0.1	−40.5	0.1
trans-HONN(O)H	**10**	*trans*-ON(H)NO$^-$	**5**	−16.3	4.4	−16.9	4.2
trans-HONN(O)H	**10**	*trans*-HONNO$^-$	**15**	−40.3	0.2	−40.9	0.1
trans-HONNOH (HRef 1)	**14**	*trans*-HONNO$^-$	**15**	0.0	7.2	0.0	7.2
cis-ON(H)NO$^-$	**4**	*cis*-ONNO^{2-}	**6**	−11.5	9.5	−9.4	9.9
cis-HONNO$^-$	**12**	*cis*-ONNO^{2-}	**6**	34.2	17.5	35.9	17.8
trans-ON(H)NO$^-$	**5**	*trans*-ONNO^{2-}	**11**	−24.0	7.4	−24.0	7.4
trans-HONNO$^-$ (HRef 2)	**15**	*trans*-ONNO^{2-}	**11**	0.0	11.5	0.0	11.5

two possible sites for O-protonation, for *trans*, both intermediates (**9**, **10**) are equally feasible, whereas *cis*-HONN(O)H (**7**) is energetically more favorable than *cis*-HON(H)NO (**8**). In addition, a fast intramolecular hydrogen transfer between the oxygen atoms is possible, resulting in equilibration of the *cis* species (**7** and **8**). A further deprotonation step yields the single protonated hyponitrite (**12**, **15**). Similarly, under moderate *alkaline* conditions, the formation of singly protonated hyponitrite (**12**, **15**) is predicted to proceed through **6** and **11** via sequential deprotonation and protonation. Whereas the *trans*-hyponitrite anion (**15**) will be easily protonated under acidic conditions, single protonated *cis*-hyponitrite (**12**) is the dominant species down to a pH of 3.1 and, due to a high p$K_{a,2}$ value of 17.5, is stable under alkaline conditions with respect to deprotonation as well. Both *cis* species (**12**, **13**) and the *trans*-hyponitrite anion (**15**) are considered to be unstable and decompose to form the final product N_2O with relatively low activation barriers of 42, 73, and 84 kJ/mol, respectively. These calculated barriers are in accordance with the literature values for the *cis* isomers but are somewhat lower than the experimental value of 98 kJ/mol reported for the *trans* isomer decomposition.[30,37,38] Note that *trans*-hyponitrous acid (**14**) is fairly stable in solution due to the absence of a feasible intramolecular elimination channel. In summary, under acidic conditions the following reaction sequences are possible:

$$trans-\mathrm{ON(H)N(H)O}\ (\mathbf{3}) \rightleftharpoons \mathbf{5} \rightleftharpoons \mathbf{9} \rightleftharpoons \mathbf{15} \rightleftharpoons trans-\mathrm{HONNOH}\ (\mathbf{14}) \quad (12)$$

$$\rightleftharpoons \mathbf{5} \rightleftharpoons \mathbf{9} \rightleftharpoons \mathbf{15} \rightarrow \mathrm{N_2O} + \mathrm{H_2O}\ (\mathbf{16}) \quad (13)$$

$$\rightleftharpoons \mathbf{5} \rightleftharpoons \mathbf{9} \rightleftharpoons \mathbf{8} \rightleftharpoons \mathbf{12} \rightarrow \mathrm{N_2O} + \mathrm{H_2O}\ (\mathbf{16}) \quad (14)$$

$$cis-\mathrm{ON(H)N(H)O}\ (\mathbf{2}) \rightleftharpoons \mathbf{4} \rightleftharpoons \mathbf{7} \rightleftharpoons \mathbf{12} \rightarrow \mathrm{N_2O} + \mathrm{H_2O}\ (\mathbf{16}) \quad (15)$$

$$\rightleftharpoons \mathbf{4} \rightleftharpoons \mathbf{7} \rightleftharpoons \mathbf{12} \rightleftharpoons \mathbf{13} \rightarrow \mathrm{N_2O} + \mathrm{H_2O}\ (\mathbf{16}) \quad (16)$$

Hence, the formation of N_2O is attributed to the species *cis*-HONNO$^-$ (**12**), *cis*-HONNOH (**13**), and *trans*-HONNO$^-$ (**15**). Due to lower activation barriers and in agreement with the already mentioned destabilizing orbital interactions (see section 3.3), the *cis* species are kinetically more unstable than the *trans*-hyponitrite anion. Decomposition of the *trans* species, in agreement with experiments, is rather slow.

cis and trans Pathways. As in the intramolecular reaction scheme, the *cis* and the *trans* pathway are well isolated. The only possible isomerization that might compete with the fast acid−base equilibria takes place between **8** and **9**. This equilibrium is in favor of the *cis* isomer and, therefore, could enable another pathway toward *cis*-hyponitrite. However, deprotonation of **9** and **10** can be estimated to proceed with a rate constant on the order of 10^{10} s^{-1} (as derived from the pK_a value by assuming a diffusion controlled protonation reaction). This is several orders of magnitude higher than a rough estimate of the isomerization reaction rate constant on the order of 1 s^{-1}, which is based on the free enthalpy of activation given in Table 2. Therefore, it appears unlikely that isomerization contributes significantly, and two well-separated *cis* and *trans* pathways can be assumed. Keeping in mind the strongly favored initial *cis* dimer formation (section 3.1), it becomes clear that the overall reaction is dominated by the *cis* pathway.

On the *cis* pathway, formation of the *cis*-hyponitrite anion (**12**) can be assumed to be rapid. Taking into account the high thermodynamic stability (due to the strong intramolecular hydrogen bonding, section 3.3) and the kinetic destabilization (due to the population of the σ^*(N−O) orbitals, section 3.3), decomposition of the *cis*-hyponitrite anion (**12**) will be preferred over the protonation equilibrium between **12** and **13** and subsequent decomposition of *cis*-hyponitrous acid (**13**). Therefore, N_2O formation from **12** dominates over almost the entire pH range and contributions of the molecular *cis*-hyponitrous acid pathway only become significant at very low pH values.

For the minor *trans* pathway, the model predicts the formation of the moderately stable *trans*-HONNOH (**14**) in the acidic range around pH = 0. With increasing pH, the equilibration with the monoanion (**15**) becomes significant and a slow decomposition sets in. At higher pH, the equilibrium is moved to the side of the

stable dianion and the decomposition rate decreases again. Thus, the rate of the *trans*-decomposition is predicted to be slow and strongly pH dependent following the bell-shaped curve found experimentally by Buchholz and Powell.[38]

In summary, we conclude that the major pathway of nitrous oxide formation from HNO dimerization follows a sequence of rapid heterolytic bond cleavages according to eq 15, which is completed with the decomposition of the *cis*-hyponitrite anion (**12**) to form N_2O.

3.5. Assessment of the Acid−Base Equilibrium Model. The acid−base equilibrium model, in contrast to the formerly discussed intramolecular model, provides a theoretically sound framework for the formation of N_2O from HNO dimerization and *trans*-$HONNO^-$ decomposition. As a further check of its consistency, the model must be capable of explaining previous experimental results. In the following, with a focus on the equilibrium of the intermediate *cis*-hyponitrous acid, (i) experimental results of the HNO dimerization reaction at varying pH values taken from the literature and (ii) spectroscopic measurements concerning the formation of OH radicals are compared with model predictions. Finally, the role of NO^- for dimerization in highly alkaline solutions and the reason for the distinct differences between the acid−base characteristics of the *cis* and *trans* isomers will be addressed.

HNO Dimerization Experiments. Several experimental studies with reactions taking place under acidic, neutral, and moderate alkaline conditions are reported that include HNO dimerization to explain N_2O formation.[1,17,39] In the following, the outcomes of three selected studies performed in different pH ranges are analyzed with respect to the applicability of the acid−base equilibrium model and to support the predicted *cis*-preference of the initial HNO dimerization step:

Under *acidic* conditions (pH = 1), according to Bell and Kelly,[17] selective reduction of sodium nitrite yields nitroxyl. Utilizing trimethylamine borane (TMAB) as hydride donor in water−dioxane (the latter preventing a possible radial chain reaction observed in this pH region[40]), the corresponding HNO forming reaction has been postulated to be

$$H_2NO_2^+ + H^-(\text{from TMAB}) \rightarrow HNO + H_2O \quad (17)$$

Assuming the validity of our mechanism, under these strongly acidic conditions, HNO dimerization could take place through the pathways given by eqs 12, 15, and 16 with **12**, **13**, and **14** as the intermediate products. As outlined above, at pH = 1 both *cis* species **13** and **12** may contribute to nitrous oxide formation. In contrast, the formed *trans*-hyponitrous acid (**14**) was found to be stable[38] or possibly reacts with available nitrite to yield N_2.[40] In fact, Bell and Kelly reported fast and almost stoichiometric transformation of nitrite into nitrous oxide (1.92:1). From this it follows that only traces of **14** have been formed in the reaction, thus in agreement with our prediction of a preference for the *cis* pathway.

However, a chance of misinterpretation of the reaction sequence remains, because it cannot be completely ruled out that certain amounts of NO are formed from nitrous acid (HONO) disproportionation as byproduct as well. NO reacts rapidly with HNO, and the subsequent chain reaction of the product leads to the formation of *trans*-$N_2O_2H_2$ and NO (at low NO concentrations) or N_2O and nitrite (at high NO concentrations).[2] Such a NO mechanism would be indistinguishable from HNO dimerization.

In *weakly acidic*, *neutral*, and *moderately alkaline* solutions, thermal decompositions of the widely used HNO donors, Angeli's salt and Piloty's acid (*N*-hydroxybenzenesulfonamide), have been extensively studied.[1] In the second case, the redetermined $pK_a = 11.4$ of the $^1HNO/^3NO^-$ equilibrium sets an upper pH limit for dimerization of HNO due to competing deprotonation.[2] After protonation of Angeli's salt ($pK_a = 9.7$) and deprotonation of Piloty's acid ($pK_a = 9.3$), the decompositions of the two anions follow first-order kinetics with similar rate constants ($6.8 \times 10^{-4}\ s^{-1}$ and $4 \times 10^{-4}\ s^{-1}$)[18,41] over a wide pH range according to

$$ON(H)NO_2^- \rightleftharpoons NO_2^- + HNO \quad (pH = 4-8) \quad (18)$$

$$PhSO_2NHO^- \rightleftharpoons PhSO_2^- + HNO \quad (pH > 11) \quad (19)$$

On the basis of the presented acid−base scheme, consecutive reactions according to eqs 13 and 15 (via **6** and **11** under alkaline conditions) will lead to **12** and **15** as possible nitrous oxide producing species. The corresponding *cis* pathway includes the rapid decomposition of **12** and is consistent with the reported pH independent rate constants. In contrast to the *cis* isomer (**12**), which is the dominant species at $3.1 < pH < 17.5$, the *trans* isomer **15** equilibrates with the stable *trans*-species (**11**, **14**). According to the measurements of Buchholz and Powell, the effective decomposition rate constant of **15** decreases from its maximum value, $5 \times 10^{-4}\ s^{-1}$ at pH = 9, to $<1 \times 10^{-5}\ s^{-1}$ at pH = 4 and $3 \times 10^{-5}\ s^{-1}$ at pH = 12.[38] Thus, assuming the *trans* pathway to take place, intermediate *trans*-hyponitrite should accumulate under acidic or alkaline conditions to concentration levels that should have been detectable or should have affected the reported time-resolved UV absorption measurements. The UV spectra of *trans*-hyponitrous acid (**14**, **15**, **11**) exhibit absorption bands that are coincident with those of the reactants used for monitoring the kinetic experiment. Neither in the case of Angeli's salt[41] nor in the case of Piloty's acid[18,39] (at pH < 13) have changes of UV spectra or kinetics related to hyponitrite formation been reported, even though additional experiments designed for this purpose were performed by Seel and Bliefert.[39]

In conclusion, on the basis of kinetic and spectroscopic evidence, a reassessment of the results for all three HNO donor systems in the light of the new acid−base model reveals the absence or presence of very low amounts of *trans*-hyponitrous acid. Reaction sequences based on the *cis* dimer pathway, in agreement with our theoretical predictions, can explain the observed fast formation of nitrous oxide via final decomposition of **12** in all cases. Of course, due to the absence of possible isomerizations, these findings are also in line with the predicted initial preference of *cis* dimer formation.

Synthesis of the cis Isomers. Many early attempts of synthesizing the *cis* isomers of hyponitrous acid or its mere detection as intermediate have failed.[42] A first successful synthesis route yielding almost exclusively *cis*-hyponitrite salt was based on the reduction of NO using sodium in liquid ammonia.[43] This high selectivity with respect to the formation of the *cis* isomer is somewhat similar to the initial dimerization of HNO in water yielding preferentially the *cis*-HNO dimer. Feldmann and Jansen[44] presented another successful gas−solid phase synthesis of the *cis*-hyponitrite dianion (**6**) from N_2O and NaO. They were also able to report the first single crystal structure, which underlines the kinetic stability of *cis*-$N_2O_2^{2-}$ as a solid. However,

solvation attempts revealed that rapid decomposition of the sodium salt takes place in contact with protic solvents as well as carbon dioxide. Note that all these findings are in fact consistent with our prediction of a low acidity of the *cis* monoanion (**12**) ($pK_{a,2}$ = 17.5), which is in-between the acidities of water (15.7) and ammonia (34). Whereas *cis*-$N_2O_2^{2-}$ is stable in ammonia, fast decomposition of the single protonated species (**12**) in water gives an explanation for the former experimental problems of isolating the *cis* species in aqueous environments.

Formation of OH Radicals. It was further suggested[40] that *cis*-hyponitrous acid (**13**) is a source of OH radicals via an azo-like homolytic fission according to

$$HONNOH \rightarrow N_2 + 2OH \qquad (20)$$

Evidence for the OH radical formation has been presented in a series of EPR spin trapping studies performed by Stoyanovsky and co-workers,[6,16] and further verification of OH was found in the product yields from experiments using radical scavengers. In these studies, a pH dependent decomposition of Angeli's salt showed a maximum of OH radical formation around pH = 4. Whereas O-protonation has been shown to lead to NO formation from Angeli's salt instead of HNO at lower pH values,[36] the decrease of OH yield toward higher pH was explained by a shift of a postulated equilibrium between **13** and **8**, followed by decomposition of **8** to form nitrous oxide. Objecting to this interpretation, we find no convincing evidence for such an equilibrium. It is calculated to be thermodynamically unfavorable (pK = 5) and is definitively not pH dependent (see Figure 3). A more reasonable explanation of the results of Stoyanovsky and co-workers is the acid−base equilibrium of *cis*-hyponitrous acid (**13**), which may partly undergo homolytic fission yielding OH, and the single protonated species (**12**), which rapidly decomposes to form N_2O. The predicted pK_a value of the *cis*-hyponitrous acid equilibrium (pK_a = 3.1) fits the observed pH dependence found in the OH scavenging studies[6,16] as well as the occurrence of enhanced DNA strand breakages[5] at pH < 6 quite well.

Whereas the decomposition of the anion can easily be explained by rapid N−O bond breakage, forming N_2O and OH^-, the evaluation of the kinetic stability and the fate of the molecular *cis*-hyponitrous acid (**13**) remains difficult. Due to the significantly higher activation barrier, the intramolecular hydrogen transfer and the subsequent decomposition can be assumed to be much slower than the decomposition of the anion. Hence, the proposed azo-like homolytic fission, according to eq 20, may in fact become important. Even small amounts of generated OH radicals may serve as carriers of a chain reaction cycle forming N_2O. Note, however, that a decomposition step yielding OH most likely starts from the less stable exocyclic conformer of **13**. Therefore, it is difficult to assess the significance of such a radical process with respect to the overall N_2O formation. Furthermore, little is known about a possible O-protonation of the molecular acid (**13**) via intermolecular hydrogen transfer. Such an acid-catalyzed decomposition mechanism, which is reported[42] to be important for the isomeric *trans*-hyponitrous acid (**14**) below pH = 0, can be assumed to become relevant for the decomposition of *cis*-hyponitrous acid at low pH as well.

Dimerization in Highly Alkaline Solution. Another open question that arises from the experiments utilizing Piloty's acid is the influence of the acid−base equilibrium of HNO/NO^- on the overall dimerization process. In highly alkaline solutions, slow deprotonation of the ground state singlet ^1HNO is considered to yield the spin-forbidden triplet ground state base $^3NO^-$ rather than the spin-allowed energetically unfavorable $^1NO^-$.[2] Compared to ^1HNO, $^3NO^-$ is known to react rapidly with oxygen and nitric oxide. In this spirit, the spin-forbidden reaction of $^3NO^-$ with ^1HNO appears unlikely to be rapid in solution. However, in a recent kinetic study on photoinduced release of nitroxyl from Angeli's salt, Lymar and Shafirovich[45] came to the conclusion that this reaction might be fast as well. Attributing an unidentified $^3NO^-$ loss process exclusively to the reaction $^1HNO + {}^3NO^-$, an upper limit for the rate constant (6.6×10^9 M^{-1} s^{-1}) was reported. Moreover, at exceedingly high alkalinity, the spin-allowed dimerization of $^3NO^-$ may become significant as well, but detailed kinetic studies regarding this reaction are not available.

Following similar arguments as put forward for the kinetics of the dimerization of ^1HNO in section 3.1 it is clear that due to the different dipole moment and especially the additional charge of $^3NO^-$, quite different transition states can be expected for these reactions. Consideration of the calculated *cis*−*trans* equilibria of the possible products as given in Table 2 reveals that in the case of the reaction $^1HNO + {}^3NO^-$ a similar *cis* preference is obtained for $ON(H)NO^-$ (**4**, **5**). On the contrary, in the case of the $^3NO^-$ dimerization the *trans*-$N_2O_2^{2-}$ isomer (**11**) is calculated to be slightly more stable than the *cis*-$N_2O_2^{2-}$ isomer (**6**). Thus, it may be speculated that the isomer ratio is changed in favor of the *trans* isomer in the latter case. Indeed, evidence for the *trans*-hyponitrite dianion as a reaction product has been found in Piloty's acid decomposition experiments performed above pH > 13,[18,39] but this has previously been explained to result from a possible isomerization under alkaline conditions.[39] For sure, more experimental and theoretical studies are needed to clarify the dominant dimerization reaction in the case of the simultaneous presence of ^1HNO and $^3NO^-$.

Origin of ΔpK_a Differences. Finally, the predicted quite drastic difference between the $\Delta pK_a = pK_{a,2} - pK_{a,1}$ values of the *cis* and *trans* isomers calls for a more detailed explanation. As presented in the acid−base scheme in Figure 3, for *trans*-hyponitrous acid (**14**, **15**, **11**) ΔpK_a = 4.3 and for *cis*-hyponitrous acid (**13**,**12**,**6**) ΔpK_a = 14.4. The difference is much more pronounced than in the prominent example of maleic acid and fumaric acid, with corresponding values of ΔpK_a = 4.2 and 1.4, respectively. Following Perrin's recent discussion,[46] large ΔpK_a values do not only originate from the energetic stabilization resulting from intramolecular hydrogen bonding but are also an effect of preventing electrostatic "strain" arising from the proximity of the charged heteroatoms in the dianion. Whereas in most organic molecules certain structural adaptions can reduce this effect, in the case of the *cis*-hyponitrite dianion (**6**) the partial double bond character of the N−N bond leads to a fixation of the unfavorable structure. Thus, an evasion into a nonplanar structure as well as a further increase of the N−N distance are energetically demanding. The first protonation will therefore not only enable formation of an energetically favorable hydrogen bond but also remove the electrostatic destabilization and enable relaxation of the "strained" structure. The corresponding high proton affinity of the dianion is in accordance with a pronounced shift of the $pK_{a,2}$ toward a higher value.

The second protonation results in the uncharged *cis*-hyponitrous acid (**13**), which shows no pronounced hydrogen bonding, as evident from the low energy differences of the corresponding *cis*-conformers calculated already by Zevallos et al.[34] for the gas

phase species. This pronounced difference of the intramolecular hydrogen bonding energy compared to the monoanion (**12**) gives an explanation for the shift of the $pK_{a,1}$ toward a lower value.

Taking together the effect of electrostatic "strain" and hydrogen bonding, this gives an explanation of the unique ΔpK_a difference between the *cis* and the *trans* isomers.

4. CONCLUSION

Two different DFT based models for N_2O formation from HNO dimerization were analyzed regarding their potential to explain the quite complex experimental results for N_2O formation in solution. In contrast to the previously recommended intramolecular rearrangement scheme, a fast acid−base equilibria based mechanism is in agreement with experimental findings. According to our mechanism, N_2O formation is dominated by initial formation of the *cis*-HNO dimer, followed by rapid proton transfer reactions and finally decomposition of the *cis*-hyponitrite anion. A minor formation (if any) of the *trans*-HNO dimer leads to the formation of *trans*-hyponitrous acid, which slowly decays via the corresponding anion. Theoretically calculated pK_a values revealed an enhanced stability of the *cis*-hyponitrite anion due to the formation of an intramolecular hydrogen bond and a strictly deviating acid−base chemistry of the *cis* and the *trans* isomers. Under physiological conditions, the decomposition of the *cis*-hyponitrite anion should dominate the formation of nitrous oxide, whereas at low pH (<4) various decomposition mechanisms of the uncharged species may become relevant. Specifically designed experiments are needed to further test our new mechanism. Currently, experiments on isotope selective detection of N_2O are underway that help to differentiate between alternative reaction pathways.

■ ASSOCIATED CONTENT

Supporting Information. All calculated structures and energies. This material is available free of charge via the Internet at http://pubs.acs.org.

■ AUTHOR INFORMATION

Corresponding Author
fehling@phc.uni-kiel.de; friedrichs@phc.uni-kiel.de

■ ACKNOWLEDGMENT

The authors thank Douglas W. R. Wallace for encouraging us to take a closer look at N_2O formation mechanisms and two anonymous reviewers for their detailed comments. Financial support by the German Science Foundation (DFG-EC80) in the framework of the cluster of excellence "The Future Ocean" is gratefully acknowledged.

■ REFERENCES

(1) Miranda, K. M. *Coord. Chem. Rev.* **2005**, *249*, 433–455.
(2) Shafirovich, V.; Lymar, S. V. *Proc. Natl. Acad. Sci. U. S. A.* **2002**, *99*, 7340–7345.
(3) Bartberger, M. D.; Liu, W.; Ford, E.; Miranda, K. M.; Switzer, C.; Fukuto, J. M.; Farmer, P. J.; Wink, D. A.; Houk, K. N. *Proc. Natl. Acad. Sci. U. S. A.* **2002**, *99*, 10958–10963.
(4) Paolocci, N.; Jackson, M. I.; Lopez, B. E.; Miranda, K.; Tocchetti, C. G.; Wink, D. A.; Hobbs, A. J.; Fukuto, J. M. *Pharmacol. Ther.* **2007**, *113*, 442–458.
(5) Ohshima, H.; Gilibert, I.; Bianchini, F. *Free Radical Biol. Med.* **1999**, *26*, 1305–1313.
(6) Ivanova, J.; Salama, G.; Clancy, R. M.; Schor, N. F.; Nylander, K. D.; Stoyanovsky, D. A. *J. Biol. Chem.* **2003**, *278*, 42761–42768.
(7) Sulc, F.; Farmer, P. J. *The smallest biomolecules: diatomics and their interactions with heme proteins*; Elsevier Science: 2008; pp 429−462.
(8) Kohout, F. C.; Lampe, F. W. *J. Am. Chem. Soc.* **1965**, *87*, 5795–5796.
(9) Smith, P. A. S.; Hein, G. E. *J. Am. Chem. Soc.* **1960**, *82*, 5731–5740.
(10) Bazylinski, D. A.; Hollocher, T. C. *J. Am. Chem. Soc.* **1985**, *107*, 7982–7986.
(11) Akhtar, M. J.; Balschi, J. A.; Bonner, F. T. *Inorg. Chem.* **1982**, *21*, 2216–2218.
(12) Lin, M. C.; He, Y.; Melius, C. F. *Int. J. Chem. Kinet.* **1992**, *24*, 489–516.
(13) Bryukov, M.; Kachanov, A.; Timonnen, R.; Seetula, J.; Vandoren, J.; Sarkisov, O. *Chem. Phys. Lett.* **1993**, *208*, 392–398.
(14) Ruud, K.; Helgaker, T.; Uggerud, E. *J. Mol. Struct.* **1997**, *393*, 59–71.
(15) Lüttke, W.; Skancke, P. N.; Traetteberg, M. *Theor. Chem. Acc.* **1994**, *87*, 321–333.
(16) Stoyanovsky, D. A.; Clancy, R.; Cederbaum, A. I. *J. Am. Chem. Soc.* **1999**, *121*, 5093–5094.
(17) Bell, K. E.; Kelly, H. C. *Inorg. Chem.* **1996**, *35*, 7225–7228.
(18) Bonner, F. T.; Ko, Y. *Inorg. Chem.* **1992**, *31*, 2514–2519.
(19) Frisch, M. J.; et al. *Gaussian 09*, Revision A.02; Gaussian Inc.: Wallingford, CT, 2009.
(20) Dunning, T. H. *J. Chem. Phys.* **1989**, *90*, 1007–1023.
(21) Tomasi, J.; Mennucci, B.; Cammi, R. *Chem. Rev.* **2005**, *105*, 2999–3094.
(22) Ho, J.; Coote, M. L. *J. Chem. Theory Comput.* **2009**, *5*, 295–306.
(23) Bonner, F. T.; Hughes, M. N. *Comments Inorg. Chem.* **1988**, *7*, 215–234.
(24) Marenich, A. V.; Cramer, C. J.; Truhlar, D. G. *J. Phys. Chem. B* **2009**, *113*, 6378–6396.
(25) Glaser, R.; Murmann, R. K.; Barnes, C. L. *J. Org. Chem.* **1996**, *61*, 1047–1058.
(26) Peters, N. J. S. *J. Phys. Chem. A* **1998**, *102*, 7001–7005.
(27) Callear, A. B.; Carr, R. W. *J. Chem. Soc., Faraday Trans.* **1975**, *71*, 1603–1609.
(28) Connors, K. *Chemical kinetics: the study of reaction rates in solution*; Wiley-VCH: 1990.
(29) Kirkwood, J. G. *J. Chem. Phys.* **1934**, *2*, 351–361.
(30) Ashcraft, R. W.; Raman, S.; Green, W. H. *J. Phys. Chem. A* **2008**, *112*, 7577–7593.
(31) Raman, S.; Ashcraft, R. W.; Vial, M.; Klasky, M. L. *J. Phys. Chem. A* **2005**, *109*, 8526–8536.
(32) Hussain, M. A.; Stedman, G.; Hughes, M. N. *J. Chem. Soc. B* **1968**, 597–603.
(33) Loechler, E. L.; Schneider, A. M.; Schwartz, D. B.; Hollocher, T. C. *J. Am. Chem. Soc.* **1987**, *109*, 3076–3087.
(34) Zevallos, J.; Toro-Labbé, A.; Mó, O.; Yáñez, M. *Struct. Chem.* **2005**, *16*, 295–303.
(35) Musin, R. N.; Mariam, Y. H. *J. Phys. Org. Chem.* **2006**, *19*, 425–444.
(36) Dutton, A. S.; Fukuto, J. M.; Houk, K. N. *J. Am. Chem. Soc.* **2004**, *126*, 3795–3800.
(37) Hammerl, A. Hochenergetische, stickstoffreiche Verbindungen. Ph.D. Thesis, 2001.
(38) Buchholz, J. R.; Powell, R. E. *J. Am. Chem. Soc.* **1963**, *85*, 509–511.
(39) Seel, F.; Bliefert, C. *Z. Anorg. Allg. Chem.* **1972**, *394*, 187–196.
(40) Buchholz, J. R.; Powell, R. E. *J. Am. Chem. Soc.* **1965**, *87*, 2350–2353.

(41) Hughes, M. N.; Wimbledon, P. E. *J. Chem. Soc., Dalton Trans.* **1976**, 703–707.
(42) Hughes, M. N. *Q. Rev. Chem. Soc.* **1968**, *22*, 1–13.
(43) Goubeau, J.; Laitenberger, K. *Z. Anorg. Allg. Chem.* **1963**, *320*, 78–85.
(44) Feldmann, C.; Jansen, M. *Z. Anorg. Allg. Chem.* **1997**, *623*, 1803–1809.
(45) Lymar, S. V.; Shafirovich, V. *J. Phys. Chem. B* **2007**, *111*, 6861–6867.
(46) Perrin, C. L. *Acc. Chem. Res.* **2010**, *43*, 1550–1557.